Brain tumor visualization for magnetic resonance images using modified shape-based interpolation method

Dina Mohammed Sherif El-Torky[1], Mohamed Ismail Roushdy[2], Maryam Nabil Al-Berry[1], Mohammed Abd El-Megeed Salem[3]

[1]Faculty of Computer and Information Sciences, Ain Shams University, Cairo, Egypt
[2]Faculty of Computers and Information Technology, Future University in Egypt, Cairo, Egypt
[3]Faculty of Media Engineering and Technology, German University in Cairo, Cairo, Egypt

Article Info

ABSTRACT

3D visualization plays an essential role in medical diagnosis and setting treatment plans especially for brain cancer. There have been many attempts for brain tumor reconstruction and visualization using various techniques. However, this problem is still considered unsolved as more accurate results are needed in this critical field. In this paper, a sequence of 2D slices of brain magnetic resonance Images was used to reconstruct a 3D model for the brain tumor. The images were automatically segmented using wavelet multi-resolution expectation maximization algorithm. Then, the inter-slice gaps were interpolated using the proposed modified shape-based interpolation method. The method involves three main steps; transferring the binary tumor images to distance images using a suitable distance function, interpolating the distance images using cubic spline interpolation and thresholding the interpolated values to get the reconstructed slices. The final tumor is then visualized as a 3D isosurface. We evaluated the proposed method by removing an original slice from the input images and interpolating it, the results outperform the original shape-based interpolation method by an average of 3% reaching 99% of accuracy for some slice images.

This is an open access article under the CC BY-SA license.

Corresponding Author:

Dina Mohammed Sherif El-Torky
Faculty of Computer and Information Sciences, Ain Shams University
Al-Khalifa Al-Maamoun St., Abbassiya, Cairo, Egypt
Email: dina.eltorky@cis.asu.edu.eg

1. INTRODUCTION

Brain cancer is one of the most life-threatening diseases to human beings. More than 22,000 people in the United States of America are diagnosed with brain tumors every year [1]. The treatment process involves one or more of surgical resection, radiotherapy, and chemotherapy. For the oncologist to decide a suitable treatment plan, there must be an accurate and reliable diagnosis of the pathology, location, shape, and size of the tumor. The diagnostic techniques are mainly divided into invasive techniques, e.g., biopsy, and non-invasive techniques such as medical imaging tools.

Magnetic resonance imaging (MRI) is an important imaging tool for medical diagnosis especially for lesions. The images can show the lesion properties when injecting the patient with Gadolinium-based contrast agent [2]. However, the MRI yields a set of cross-sectional 2D images that need further interpretation from an expert radiologist to construct a 3D model of the tumor from these slices. This can result in an inaccurate diagnosis because the analysis depends on the experience of the radiologist [3]–[5]. Moreover, to avoid the slices from interference with each other (crosstalk artifacts), there must be an inter-

slice spacing during the image acquisition [6] which causes loss of details in the gap spaces and extra effort from the radiologist to analyse the images.

As a result, many attempts are being made to provide an automated visualization for brain tumors. We propose a modified shape-based interpolation technique to estimate the missing information in the gap slices then reconstruct a 3D model of the tumor that can be easily viewed and interpreted. First, the tumor is segmented from each MRI slice. Then the tumor images are converted to distance images which are used to interpolate the in-between missing slices. Finally, the tumor volume is rendered and displayed in a 3-D view.

The rest of the paper is organized; section 2 reviews the most popular methods that are currently used for tumor 3D reconstruction. Section 3 explains the methods used for tumor segmentation and extraction. The proposed method is presented in section 4. Results are shown in section 5 and the conclusions are demonstrated in section 6.

2.   RELATED WORK

3D reconstruction is implemented using various methods that are based on diverse concepts. In this section, we will discuss the most widely-used methods [3].

2.1. Delaunay and alpha-shapes

Delaunay methods are mainly based on extracting tetrahedron surfaces from an initial point cloud. The concept of 3D reconstruction using alpha-shapes was first introduced by Edelsbrunner and Mucke [7]. Using a finite set of points S and the parameter alpha, the resulting alpha-shape of S is a polytope, which is a generalization in any number of dimensions, of the three-dimensional polyhedron that is not necessarily convex or connected. If the alpha value is large, the alpha shape of S is similar to its convex hull. By decreasing the value of alpha, the non-convex details of the shape are formed. Edelsbrunner and Mucke [7] modified the technique by forming a surrounding sphere smaller than alpha then removing all tetrahedrons that lie inside it. External triangles of the remaining tetrahedron form the final surface. Al-Tamimi *et al.* [8] used alpha-shape theory for 3D reconstruction of brain tumors using slices of MR images. Most delaunay-based methods have the advantage of accurately fitting the surface defined by the original point cloud. On the other hand, their performance is strongly affected with noise.

2.2. Zero-set methods

Zero-set methods are also known as implicit reconstruction methods. They use a distance function for surface reconstruction. A polygonal representation of the object is formed by extracting a zero-set using a contour algorithm. Therefore, surface reconstruction from a point cloud is simplified to computing the suitable function f which equals zero for the sampled points and does not equal zero for the rest of the points [3]. The most popular zero-set method is the marching cubes algorithm which was proposed by Lorensen and Cline [9]. Guo *et al*. [10] introduced an improved marching cube algorithm by combining the seeded region growing and the standard Monte Carlo (MC) algorithm. Many other methods were proposed based on Zero-set methods such as Kazhdan and Hoppe [11] and Walder *et al.* [12] The drawback of these methods is the loss of geometrical accuracy in high-curvature areas such as corners and edges of the re-constructed shape.

2.3. Point-based methods

From the popular point-based methods is the voxel-grid filtering. It is based on the idea of reducing the number of points by sampling the input space using a grid of 3D voxels then a centroid is selected for each voxel to represent all the points [13], [14]. Angelopoulou *et al.* [15] used growing neural models to automatically landmark the target volume sections and construct a 3D model. The shortcoming of these methods is that it is impossible to determine the final number of points representing the surface. Methods that depend on deep learning and neural networks as in [16] and [15] were also proposed. Although that these methods produce highly efficient output, they have a drawback of finding the suitable training data especially with brain tumors that have various shapes, sizes, and consistencies.

2.4. Interpolation-based methods

To avoid interfering of slices during MRI acquisition (crosstalk artifact), there must be a gap between the images. The interpolation-based methods idea is based on calculating the image values in the gap area to reconstruct the 3D model accurately. These methods can be divided into scene-based and object-based methods. The simplest scene-based method is the linear interpolation. More methods were then proposed such as cubic spline and other polynomials in interpolation of medical images [17]. The kriging method was also used to interpolate grey values of medical images [18]. The scene-based methods apply

intensity averaging on the neighboring slices without considering the shape feature distortion. This causes blurriness to the object boundaries of the resulting interpolated slices.

Several object-based interpolation methods were proposed to avoid the shortcomings of the scene-based methods. They considered object information in the given input slices to guide the interpolation procedure. An efficient type of object-based methods is the shape-based interpolation [19], this method uses distance transform functions to build distance images from the given slices. Then, instead of interpolating the intensity values, it interpolates the displacement preserving the geometric changes of the objects more accurately. The shape-based methods have become widely used due to their efficiency. Yet, they have the problem of disability to effectively deal with object having holes, large offsets, or heavy invagination.

In [20], multi-resolution registration was used for image interpolation. Farias *et al.* [21] used interpolation techniques to generate intermediate slices of medical images. Ting *et al.* [2] applied surface reconstruction using Hermite surface interpolation for breast cancer. Our proposed method uses shape-based interpolation to estimate the intermediate gap slices of the brain tumor volume.

3. PROPOSED METHOD

Our system is based on two main processes: tumor segmentation of brain MR images and intermediate slices interpolation of binary tumor images. Various segmentation methods have been proposed throughout the past years. These methods could be very simple such as Thresholding, or region-based as region growing and watershed, or supervised classification as in artificial neural networks, or statistical-based such as expectation maximization and its modifications [22]–[26]. We used wavelet multi-resolution expectation maximization algorithm (WMEM) [27] proposed by Salem [28], [29] for tumor segmentation. Besides being an unsupervised method, WMEM showed very accurate segmentation results for the brain MR images. Figure 1 shows the process flow diagram of the proposed method.
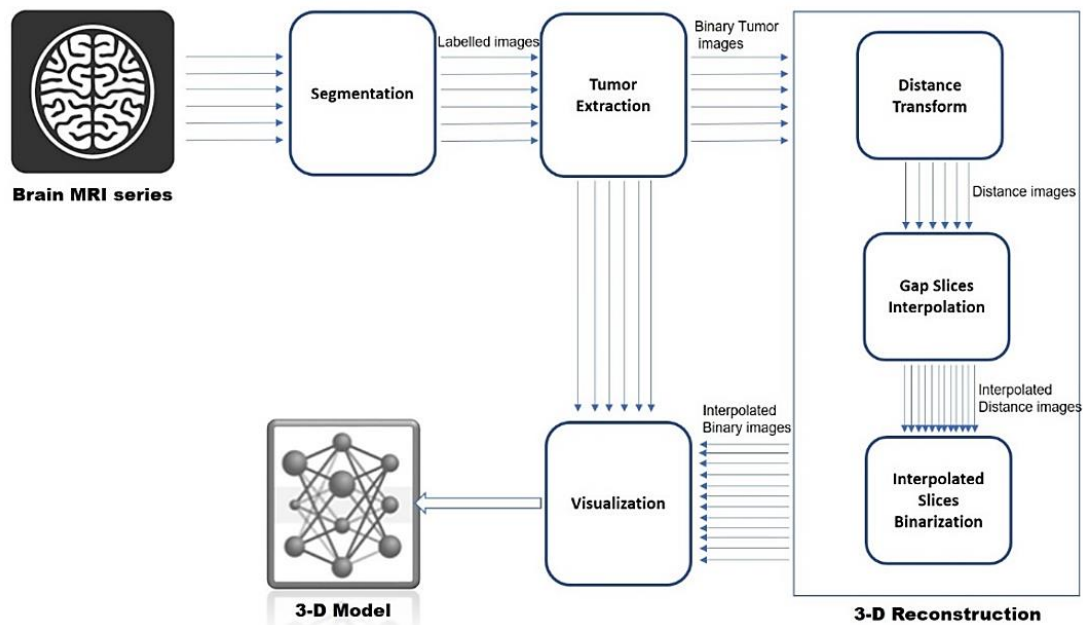

Figure 1. Process flow diagram of the proposed method

3.1. Multiresolution-based segmentation

The WMEM is basically a modification of the classic expectation maximization (EM) algorithm. The EM consists of two major steps: expectation step (E-step) and maximization step (M-step). These two steps are repeated until convergence, i.e., the difference between the parameters in the previous and the current iterations decreases until it reaches a given threshold. The EM then uses a classifier that assigns a class membership to a pixel i depending on its intensity x_i. The class to which the pixel is assigned is the one having a parameter vector that maximizes the Gaussian density function. The WMEM uses a Haar wavelet transform function that produces four outputs: image approximation, and vertical, horizontal and diagonal details of the image [30]–[32]. Two levels of approximations were produced to form a parent and a

grandparent of the original image. Since the edge details are lost during formation of the parent and grandparent images, these pixels are usually misclassified.

To overcome this, a mask containing all the edges of the image is formed by adding the vertical, horizontal and diagonal details images resulted from the wavelet analysis. This mask is used to exclude the pixels laying on the edges of the image from multi-resolution segmentation. The original EM is applied on each of the original, parent and grandparent images. Each classification result is given a certain weight. Then, the final classification is calculated by combining the three weighted results as:

$$C_{(x,y)} = 0.4 * C_{0(x,y)} + 0.35 * C_{1(x,y)} + 0.25 * C_{2(x,y)}$$

where, C_0, C_1 and C_2 are the results of the classification at pixel (x,y) for the original, parent and grandparent images respectively. Figure 2 shows the segmentation results of the WMEM, Figure 2(a) the original tumor image, Figure 2(b) the original segmented image using EM, Figure 2(c) the segmented parent image, Figure 2(d) the segmented grandparent image, Figure 2(e) the final segmented image using WMEM, and Figure 2(f) the extracted tumor.

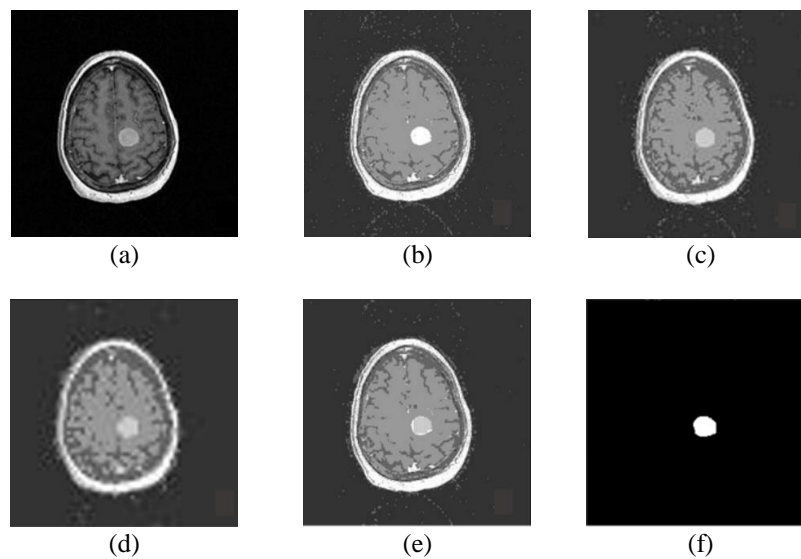|		
(a)	(b)	(c)
(d)	(e)	(f)

Figure 2. Stages of tumor extraction: (a) the original tumor image, (b) the original segmented image using EM, (c) the segmented parent image, (d) the segmented grandparent image, (e) the final segmented image using WMEM, and (f) the extracted tumor

3.2. Tumor extraction

Thresholding was used to separate the other segmented brain components (grey matter, white matter, and CSF) from the tumor. The thresholding produced images containing both tumor and skull because they almost have the same color intensity. So, the solidity feature was used to exclude the skull from the final image. Solidity is the proportion of the pixels in the convex hull that are also in the region. It is computed as Area/ConvexArea. It was found that tumors have higher solidity than the skull, so we selected the high solidity to get a binary image that only contains the tumor to be used in the reconstruction step [27].

3.3. Intermediate slice estimation

Our aim is to visualize the brain tumor given a series of MRI brain slices. Our method is a modification of the classic shape-based interpolation technique [33] which is based on interpolating the values of the 3D volume that lay in the gap areas during slices acquisition. Shape-based interpolation is performed in two main steps. The first step is transforming the binary tumor image into a distance image. The second step is interpolating the distance image using a suitable interpolation function.

Every series of MRI image is described with some important information such as the slice thickness, inter-slice distance and the in-plane resolution. These properties vary according to the MRI scanner strength and acquisition process. Before starting the interpolation, the number of gap slices should be calculated using the provided dataset properties. We computed the gap area in pixels by:

$$\frac{slice\ spacing}{in-plane\ resolution}$$

where, slice spacing is the gap between every two consecutive slices in millimeters and the in-plane resolution is the area of each pixel in millimeters [34].

3.4. Distance image transform

The distance image represents the shortest distance from every pixel in the image to the nearest boundary pixel. Pixels inside the region of interest (tumor) are assigned with positive values, while pixels of the background are assigned with negative values. We calculated the distance transform by applying the following steps twice for each of the tumor and the background separately, then the two distance images are added to form the final distance image.

Steps:

Step 1: Create two distance images D and D' for the tumor and the background respectively, then set all the pixels of D and D' to *zero*.

Step 2: Create a counter I that increments with every iteration.

Step 3: Starting from the boundary pixels, perform an erosion operation to the image to remove a single pixel from the tumor boundaries then add the value of I to the pixels of D at the locations of the eroded pixels.

Step 4: Repeat step 3 until all the pixels of D are calculated.

Step 5: Similarly, perform dilation to the tumor image by adding a single pixel starting from the boundary pixels and subtract the value of I in each iteration and insert its value in D' at the locations of the dilated pixels.

Step 6: Repeat step 5 until all the values of D' are calculated.

Step 7: By adding D to D', the final distance image is formed.

The previous steps are performed for every slice of the input volume. Figure 3 shows a sample of the distance image that results from applying the previous steps on one of our dataset images, the in-lined part represents the tumor area with positive values, while the outlined negative pixels represent the background and the zero pixels are for the tumor boundaries.
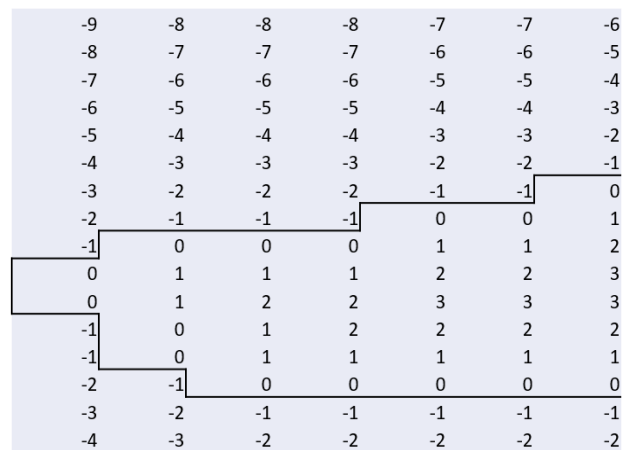
-9	-8	-8	-8	-7	-7	-6
-8	-7	-7	-7	-6	-6	-5
-7	-6	-6	-6	-5	-5	-4
-6	-5	-5	-5	-4	-4	-3
-5	-4	-4	-4	-3	-3	-2
-4	-3	-3	-3	-2	-2	-1
-3	-2	-2	-2	-1	-1	0
-2	-1	-1	-1	0	0	1
-1	0	0	0	1	1	2
0	1	1	1	2	2	3
0	1	2	2	3	3	3
-1	0	1	2	2	2	2
-1	0	1	1	1	1	1
-2	-1	0	0	0	0	0
-3	-2	-1	-1	-1	-1	-1
-4	-3	-2	-2	-2	-2	-2

Figure 3. A sample of the resulting distance image

3.5. Slice interpolation

To reconstruct the final tumor volume, the gap area has to be interpolated using the given slices. Several interpolation methods have been used in medical imaging. Methods such as nearest neighbour and linear interpolation are fast and simple, yet they do not produce reliable results [35]. In our work, B-spline interpolation [36] was used on distance images as an input, and it proved to show accurate results.

A separable spline model is chosen for interpolation. The p-dimensional spline function $s(X), X = (x_1, \dots, x_p) \in R^p$ is represented by the expansion

$$s(X) = \sum_{k \in Z^p} c(k) \varphi(X - k) \tag{1}$$

where, $c(k)$ are the B-spline coefficients. The basis functions in (1) are the integer shifts of the separable B-spline $\varphi(X)$, which is a tensor product of the univariate B-splines of degree n:

$$\varphi(X) = \beta^n(x_1) \dots \beta^n(x_p) \tag{2}$$

From the fold convolution of the box function, we can obtain the univariate B-splines. Their closed form expression is:

$$\beta^n(x) = \frac{\Delta^{n+1} x_+^n}{n!} \tag{3}$$

where, $x_+^n = \max\{0, x\}^n$ is the one-sided power function and Δ^{n+1} is the $(n+1)$ iteration of the central finite difference operator $\Delta f(x) = f\left(x + \frac{1}{2}\right) - f(x - \frac{1}{2})$. For a multidimensional image array $f(i), i \in Z^p$, the basic interpolation problem is to determine the coefficients c(k) in (1) such that the spline $S(X)$ fits the pixel values exactly: $S(X)|_{x=i} = f(i), i \in Z^p$. By applying this constraint and resampling (1) at the integers we get:

$$f(i) = \sum_{k \in Z^p} c(k) \varphi(i - k). \tag{4}$$

Since (4) has the form of discrete convolution, we can determine the $c(k)$ values by deconvolving the equation. In this study, experimental results showed that cubic spline interpolation proved to have higher accuracy than many interpolation methods such as linear, cubic and Hermite-splines.

3.6. Interpolated slice binarization

After applying interpolation on the input distance images of the tumor slices, the resulting interpolated distance images must be converted to binary images so that the gap slices can be inserted accurately. That was simply done be assigning all the zero and positive values to one (representing the tumor area) and zero to all the negative values (representing the background). By analyzing the results of shape-based interpolation, it was found that the interpolated image is always smaller than the ground truth image (i.e., the majority of error is produced as false negative pixels). This happens due to assigning all the interpolated negative values as background pixels, even if their value is very small. To overcome this drawback, we added a thresholding step to approximate the negative values so that they are not considered as background. The threshold was selected upon experimental trials. This modification improved the accuracy of the original method for all the used dataset images.

3.7. Visualization

After interpolating all the intermediate slices for the whole tumor images, the original and interpolated slices are stacked to form a 3D volume. Then, Isosurface is extracted and displayed in a 3-dimensional view. Figure 4 shows the visualized brain tumor before slices interpolation, while Figure 5 shows the visualized tumor using slices interpolation. It is noticed that the details of the tumor shape are displayed clearly after applying the proposed method.
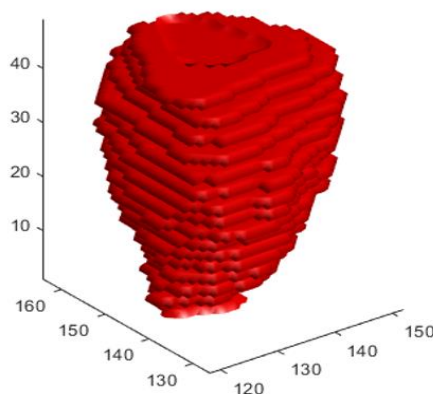

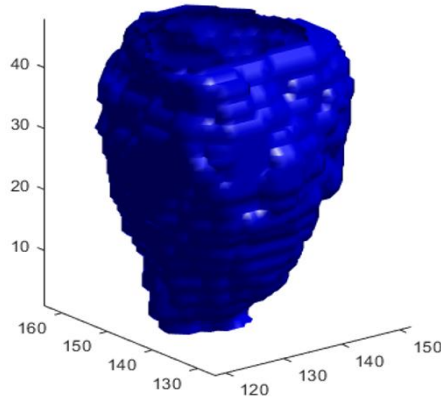Figure 4. Displayed tumor volume without interpolation

Figure 5. The displayed interpolated tumor volume

4.   RESULTS AND DISCUSSION

Data from the Internet brain segmentation repository (IBSR) was used in this study [37] which is provided by the Center for Morphometric Analysis at Massachusetts General Hospital. The data consists of multiple brain MRI scans for a patient with a tumor taken at roughly 6-month intervals over three and a half years. The algorithm was implemented using MATLAB® R2017b. Table 1 demonstrates the properties of the used MRI images series.

As the provided data does not contain ground truth values, the system accuracy was calculated by removing an original slice from the MRI images, then interpolating it. The interpolated image was then compared with the original removed image and the percent error was computed as (5):

$$\delta = \frac{|OA - IA|}{OA} \times 100 \tag{5}$$

where, OA is the area of the object cross section in the removed slice and IA is the area of the object cross section in the interpolated slice. We compared our method with the original shape-based interpolation proposed by Raya and Udupa [33] and with Hermite interpolation used in [2].

The results are summarized in Tables 2 to 5. The results represent the accuracy percentage for each slice which is computed as $100 - \delta$, where δ is the error percentage mentioned in (5). The first and last slices were excluded from the computations because for reliable interpolation results, the query points should lie in between the control points [33].

Table 1. Properties of the used MRI images series

Series no.	No. of slices with tumor	Slice Spacing (mm)	In-plane Resolution
126_10	17	3	1.015625
126_13	16	2.5	1.015625
126_21	17	2.5	0.937500
126_26	17	0	0.937500

Table 2. Accuracy percentage for each interpolated slice for series 126_10 of IBSR dataset

Slice no.	Original shape-based	Hermite interp.	Modified shape-based interp.
2	83.8	88.2	92.1
3	84.0	91.2	92.7
4	85.8	86.6	91.6
5	86.3	88.3	91.9
6	90.0	92.4	95.0
7	87.9	91.5	93.4
8	90.8	92.2	94.6
9	86.6	89.2	94.5
10	88.1	91.1	93.9
11	88.4	91.3	95.7
12	88.2	89.6	94.8
13	86.6	88.0	92.0
14	85.5	90.4	93.6
15	83.9	91.1	94.9
16	83.5	92.7	95.2

Table 3. Accuracy percentage for each interpolated slice for series 126_13 of IBSR dataset

Slice no.	Original shape-based	Hermite interp.	Modified shape-based interp.
2	79.2	81.4	86.7
3	80.1	90.6	91.6
4	81.3	88.0	92.3
5	86.5	92.1	94.1
6	87.0	92.1	94.3
7	88.7	92.1	94.6
8	88.8	94.9	96.0
9	87.7	91.0	95.8
10	88.7	95.0	96.1
11	88.6	90.7	94.7
12	89.7	94.8	96.8
13	87.6	89.8	92.9
14	81.4	83.2	90.0
15	79.1	84.6	89.9
mean ±variance	85.31±16.53	90.02±18.50	93.27±8.382

Table 4. Accuracy percentage for each interpolated slice for series 126_21 of IBSR dataset

Slice no.	Original shape-based	Hermite interp.	Modified shape-based interp.
2	83.3	87.6	92.4
3	83.0	85.5	91.6
4	84.7	87.6	92.1
5	86.3	91.9	92.6
6	92.3	94.5	96.0
7	92.8	96.2	97.1
8	90.9	93.9	96.2
9	92.4	93.0	95.9
10	89.6	90.5	93.8
11	90.0	89.5	92.8
12	91.7	95.6	97.4
13	88.6	88.9	95.9
14	92.1	95.9	97.0
15	89.2	91.5	93.9
16	81.7	85.8	89.7
mean ±variance	88.57±14.556	91.19±13.19	94.29±5.629

Table 5 Accuracy percentage for each interpolated slice for series 126_26 of IBSR dataset

Slice no.	Original shape-based	Hermite interp.	Modified shape-based interp.
2	83.4	88.9	92.2
3	89.4	90.7	93.9
4	90.4	91.4	94.5
5	91.3	92.0	95.6
6	89.8	92.3	95.8
7	89.6	93.7	95.6
8	87.9	91.4	94.9
9	92.9	94.2	97.1
10	93.0	95.2	97.7
11	92.2	93.8	96.7
12	92.8	93.6	96.1
13	90.5	93.4	95.8
14	91.4	93.2	95.9
15	90.6	93.1	96.3
16	85.7	89.9	92.7
mean ±variance	90.06±7.248	92.45±2.987	95.38±2.33

The final accuracy of the interpolated tumor volume is expected to be higher than the accuracy of the previous results. As when removing an original slice, the distance between the given slices (i.e., control points) is doubled, which will eventually decrease the interpolation accuracy. It was also noticed in Figure 6 that the error pixels are distributed evenly around the tumor boundary, Figure 6(a) the original tumor image, Figure 6(b) the interpolated tumor image, and Figure 6(c) the difference between A and B, green pixels represent the false positives and red pixels represent the false negatives. We used the structural similarity index (SSIM) to compare the interpolated and the original images. SSIM tells how much one image is structurally similar to the other [38], [39]. Values between 98% and 99% were gained. This shows that the interpolated tumor preserved its original shape and curvature areas, which will not affect the medical analysis of the system output. Since no automatic method has yet been proved to be reliable for usage as ground truth,

human expertise is still needed to confirm the efficiency of the automatic methods [40]. We contacted some experts in the Neurosurgical department of Ain Shams University, and they approved the reliability and efficiency of the reconstructed tumor images.

(a)   (b)   (c)
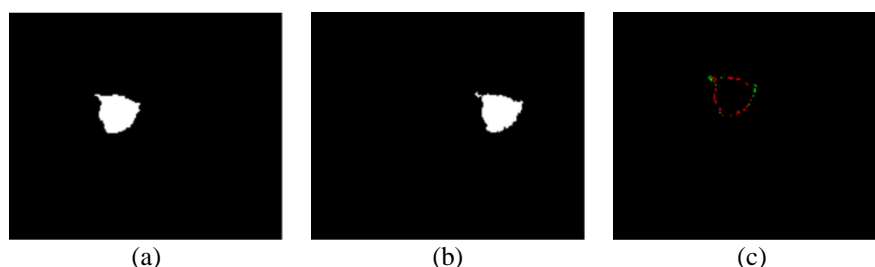
Figure 6. Difference between original and interpolated tumor images, (a) the original tumor image, (b) the interpolated tumor image, and (c) the difference between a and b, green pixels represent the false positives and red pixels represent the false negatives

5. CONCLUSION

Brain tumor visualization can efficiently help in treatment planning and resection assessment of brain cancer. Having accurate information about the shape and size of the tumor will increase the chances of total resection, which will eventually increase the mean survival period of the patient. Many attempts have been done for brain tumor visualization using different methods such as alpha-shapes, marching cubes, point-based methods, and interpolation-based methods.

In this paper, we presented a modified shape-based interpolation method for 3D reconstruction of brain tumors using a group of parallel MRI image slices. The tumor was first segmented from each brain slice using the WMEM algorithm, then the gap area was computed using our method. The final 3D shape of tumor was then displayed using isosurface function. The accuracy of the system was calculated by removing an original slice from the series and interpolating it, then comparing both images. An average accuracy of 94.1% was gained when comparing the images pixel by pixel, while the average SSIM was 98.5% which reveals that the proposed method preserves the structural shape of the interpolated slices.

REFERENCES

[1] W. Lv, Y. Peng, C. Yang, and X. Li, "Reconstruction of brain tissue surface based on three-dimensional Tl-weighted MRI images," in *2015 8th International Congress on Image and Signal Processing (CISP)*, Oct. 2015, pp. 481–486, doi: 10.1109/CISP.2015.7407928.
[2] F. F. Ting, K. S. Sim, and Y. Lee, "Three-dimensional model reconstruction using surface interpolation with the interfacing of Hermite surface for breast cancer MRI imaging system," in *Proceedings of 2016 International Conference on Robotics, Automation and Sciences, ICORAS 2016*, 2017, pp. 1–5, doi: 10.1109/ICORAS.2016.7872625.
[3] D. M. S. El-Torky, M. N. Al-Berry, M. A.-M. Salem, and M. I. Roushdy, "3D visualization of brain tumors using MR images: a survey," *Current Medical Imaging Formerly Current Medical Imaging Reviews*, vol. 15, no. 4, pp. 353–361, Apr. 2019, doi: 10.2174/1573405614666180111142055.
[4] M. P. Arakeri and G. R. M. Reddy, "An effective and efficient approach to 3D reconstruction and quantification of brain tumor on magnetic resonance images," *International Journal of Signal Processing, Image Processing and Pattern Recognition*, vol. 6, no. 3, pp. 111–128, 2013.
[5] K. Cheng *et al.*, "Identifying radiotherapy target volumes in brain cancer by image analysis," *Healthcare Technology Letters*, vol. 2, no. 5, pp. 123–128, Oct. 2015, doi: 10.1049/htl.2015.0014.
[6] S. M. Nayak, "MRI: basic principles and applications," *Radiology*, vol. 200, no. 1, Jul. 1996, doi: 10.1148/radiology.200.1.142.
[7] H. Edelsbrunner and E. P. Mücke, "Three-dimensional alpha shapes," in *Proceedings of the 1992 workshop on Volume visualization-VVS '92*, 1992, vol. 13, no. 1, pp. 75–82, doi: 10.1145/147130.147153.
[8] M. S. Hamoud Al-Tamimi, G. Sulong, and I. L. Shuaib, "Alpha shape theory for 3D visualization and volumetric measurement of brain tumor progression using magnetic resonance images," *Magnetic Resonance Imaging*, vol. 33, no. 6, pp. 787–803, Jul. 2015, doi: 10.1016/j.mri.2015.03.008.
[9] W. E. Lorensen and H. E. Cline, "Marching cubes: A high resolution 3D surface construction algorithm," in *Proceedings of the 14th annual conference on Computer graphics and interactive techniques -SIGGRAPH '87*, 1987, vol. 21, no. 4, pp. 163–169, doi: 10.1145/37401.37422.
[10] L. Guo, M. Hu, Y. Li, W. Yan, and L. Zhao, "Three dimension reconstruction of medical images based on an improved Marching

Cubes algorithm," in *2013 6th International Conference on Biomedical Engineering and Informatics*, Dec. 2013, no. Bmei, pp. 64–68, doi: 10.1109/BMEI.2013.6746908.

[11]   M. Kazhdan and H. Hoppe, "Screened poisson surface reconstruction," *ACM Transactions on Graphics*, vol. 32, no. 3, pp. 1–13, Jun. 2013, doi: 10.1145/2487228.2487237.

[12]   C. Walder, B. Schölkopf, and O. Chapelle, "Implicit surface modelling with a globally regularised basis of compact support," *Computer Graphics Forum*, vol. 25, no. 3, pp. 635–644, Sep. 2006, doi: 10.1111/j.1467-8659.2006.00983.x.

[13]   L. Kobbelt and M. Botsch, "A survey of point-based techniques in computer graphics," *Computers and Graphics*, vol. 28, no. 6, pp. 801–814, Dec. 2004, doi: 10.1016/j.cag.2004.08.009.

[14]   C. Mineo, S. G. Pierce, and R. Summan, "Novel algorithms for 3D surface point cloud boundary detection and edge reconstruction," *Journal of Computational Design and Engineering*, vol. 6, no. 1, pp. 81–91, Jan. 2019, doi: 10.1016/j.jcde.2018.02.001.

[15]   A. Angelopoulou, A. Psarrou, J. Garcia-Rodriguez, S. Orts-Escolano, J. Azorin-Lopez, and K. Revett, "3D reconstruction of medical images from slices automatically landmarked with growing neural models," *Neurocomputing*, vol. 150, no. Part A, pp. 16–25, Feb. 2015, doi: 10.1016/j.neucom.2014.03.078.

[16]   R. Cheng *et al.*, "Deep learning with orthogonal volumetric HED segmentation and 3D surface reconstruction model of prostate MRI," in *2017 IEEE 14th International Symposium on Biomedical Imaging (ISBI 2017)*, Apr. 2017, pp. 749–753, doi: 10.1109/ISBI.2017.7950627.

[17]   T. M. Lehmann, C. Gonner, and K. Spitzer, "Survey: interpolation methods in medical image processing," *IEEE Transactions on Medical Imaging*, vol. 18, no. 11, pp. 1049–1075, 1999, doi: 10.1109/42.816070.

[18]   M. R. Stytz and R. W. Parrott, "Using kriging for 3d medical imaging," *Computerized Medical Imaging and Graphics*, vol. 17, no. 6, pp. 421–442, Nov. 1993, doi: 10.1016/0895-6111(93)90059-V.

[19]   G. T. Herman, J. Zheng, and C. A. Bucholtz, "Shape-based interpolation," *IEEE Computer Graphics and Applications*, vol. 12, no. 3, pp. 69–79, May 1992, doi: 10.1109/38.135915.

[20]   J. Leng, G. Xu, and Y. Zhang, "Medical image interpolation based on multi-resolution registration," *Computers & Mathematics with Applications*, vol. 66, no. 1, pp. 1–18, Aug. 2013, doi: 10.1016/j.camwa.2013.04.026.

[21]   F. R. Farias, P. C. Klein, R. B. Soder, J. Becker, and M. S. Pinho, "MRI interpolation for multiple sclerosis lesion quantification," in *Proceedings-International Computer Software and Applications Conference*, Jun. 2016, vol. 2, pp. 633–636, doi: 10.1109/COMPSAC.2016.159.

[22]   M. A.-M. Salem, A. Atef, A. Salah, and M. Shams, "Recent survey on medical image segmentation," in *Computer Vision*, IGI Global, 2018, pp. 129–169.

[23]   N. E. A. Khalid, M. F. Ismail, M. A. A. B. Manaf, A. F. A. Fadzil, and S. Ibrahim, "MRI brain tumor segmentation: A forthright image processing approach," *Bulletin of Electrical Engineering and Informatics*, vol. 9, no. 3, pp. 1024–1031, Jun. 2020, doi: 10.11591/eei.v9i3.2063.

[24]   S. Abdelaziz and S. Lu, "K-means algorithm with level set for brain tumor segmentation," *Indonesian Journal of Electrical Engineering and Computer Science (IJEECS)*, vol. 15, no. 2, pp. 991–1000, Aug. 2019, doi: 10.11591/ijeecs.v15.i2.pp991-1000.

[25]   N. H. I. M. Zaihani, R. Roslan, Z. Ibrahim, and K. A. F. A. Samah, "Automated segmentation and detection of T1-weighted magnetic resonance imaging brain images of glioma brain tumor," *Bulletin of Electrical Engineering and Informatics (BEEI)*, vol. 9, no. 3, pp. 1032–1037, 2020, doi: 10.11591/eei.v9i3.2079.

[26]   T. Bathini and B. Gadgay, "Hybrid enhanced ICA & KSVM based brain tumor image segmentation," *Indonesian Journal of Electrical Engineering and Computer Science (IJEECS)*, vol. 14, no. 1, pp. 478–489, Dec. 2018, doi: 10.11591/ijeecs.v14.i1.pp478-489.

[27]   D. M. S. El-Torky, M. N. Al-Berry, M. A.-M. Salem, and M. I. Roushdy, "Brain tumor segmentation using wavelet Multi-resolution expectation maximization algorithm," in *2017 Eighth International Conference on Intelligent Computing and Information Systems (ICICIS)*, Dec. 2017, vol. 2018-Janua, pp. 79–83, doi: 10.1109/INTELCIS.2017.8260030.

[28]   R. Kashyap, "Medical image segmentation and analysis," in *Advanced Classification Techniques for Healthcare Analysis*, Ain Shams University, 2019, pp. 132–160.

[29]   M. A. M. Salem and B. Meffert, "Resolution mosaic EM algorithm for medical image segmentation," in *2009 International Conference on High Performance Computing & Simulation*, Jun. 2009, pp. 208–215, doi: 10.1109/HPCSIM.2009.5192800.

[30]   S. Bajpai, H. Vikram Singh, and N. Rahman Kidwai, "3D modified wavelet block tree coding for hyperspectral images," *Indonesian Journal of Electrical Engineering and Computer Science (IJEECS)*, vol. 15, no. 2, pp. 1001–1008, Aug. 2019, doi: 10.11591/ijeecs.v15.i2.pp1001-1008.

[31]   A. Setyono and D. R. I. M. Setiadi, "Image watermarking using discrete wavelet-tchebichef transform," *Indonesian Journal of Electrical Engineering and Computer Science (IJEECS)*, vol. 16, no. 3, pp. 1416–1423, Dec. 2019, doi: 10.11591/ijeecs.v16.i3.pp1416-1423.

[32]   I. D. Irawati, S. Hadiyoso, and Y. S. Hariyani, "Multi-wavelet level comparison on compressive sensing for MRI image reconstruction," *Bulletin of Electrical Engineering and Informatics (BEEI)*, vol. 9, no. 4, pp. 1461–1467, Aug. 2020, doi: 10.11591/eei.v9i4.2347.

[33]   S. P. Raya and J. K. Udupa, "Shape-based interpolation of multidimensional objects," *IEEE Transactions on Medical Imaging*, vol. 9, no. 1, pp. 32–42, Mar. 1990, doi: 10.1109/42.52980.

[34]   J. R. Brookeman, "MRI from picture to proton," *American Journal of Roentgenology*, vol. 182, no. 3, Mar. 2004, doi: 10.2214/ajr.182.3.1820592.

[35]   G. J. Grevera and J. K. Udupa, "An objective comparison of 3-D image interpolation methods," *IEEE Transactions on Medical Imaging*, vol. 17, no. 4, pp. 642–652, 1998, doi: 10.1109/42.730408.

[36]   M. A. Unser, "Splines: a perfect fit for medical imaging," in *Medical Imaging 2002: Image Processing*, May 2002, vol. 4684, doi: 10.1117/12.467162.

[37]   NITRC, "NITRC: IBSR: tool/resource info," NITRC. 2011. http://www.nitrc.org/projects/ibsr (accessed Jan. 13, 2020).

[38]   H. Singh, *Practical machine learning and image processing*. Berkeley, CA: Apress, 2019.

[39]   A. Nagm and M. Safy, "A robust watermarking algorithm for medical images," *Indonesian Journal of Electrical Engineering and Computer Science (IJEECS)*, vol. 20, no. 3, pp. 1601–1612, Dec. 2020, doi: 10.11591/ijeecs.v20.i3.pp1601-1612.

[40]   M. Ben Abdallah, M. Blonski, S. Wantz-Mézières, Y. Gaudeau, L. Taillandier, and J.-M. Moureaux, "Relevance of two manual tumour volume estimation methods for diffuse low-grade gliomas," *Healthcare Technology Letters*, vol. 5, no. 1, pp. 13–17, Feb. 2018, doi: 10.1049/htl.2017.0013.

BIOGRAPHIES OF AUTHORS

Dina Mohammed Sherif El-Torky 🆔 Ⓖ SC Ⓟ is an Assistant Lecturer in basic sciences department and PhD student at Faculty of Computer and Information Sciences, Ain Shams University. She is specialized in medical image processing. She can be contacted at email: dina.eltorky@cis.asu.edu.eg. A list of her research activity can be found at: https://www.researchgate.net/profile/Dina_Eltorky

Mohamed Ismail Roushdy 🆔 Ⓖ SC Ⓟ he is a Professor of Computer Science and Dean of Faculty of Computers and Information Technology, Future University in Egypt, Cairo, Egypt. He is also the Former Dean of Faculty of Computer and Information Sciences, Ain Shams University, Cairo, Egypt. He can be contacted at email: Mohamed.Roushdy@fue.edu.eg. A list of his research publications can be found at: https://www.researchgate.net/profile/Mohamed_Roushdy3

Maryam Nabil Al-Berry 🆔 Ⓖ SC Ⓟ is an Assistant Professor at Scientific Computer Department, Faculty of Computer and Information Sciences, Ain Shams University. She is specialized in Machine Learning, Image Processing and Computing in Mathematics. She can be contacted at email: maryam_nabil@cis.asu.edu.eg. More about her bibliography is listed in https://www.researchgate.net/profile/Maryam_Al-berry

Mohammed Abd El-Megeed Salem 🆔 Ⓖ SC Ⓟ an Associate Professor at both Faculty of Media Engineering and Technology, German University in Cairo and Faculty of Computer and Information Sciences, Ain Shams University. He is specialized in Computing in Mathematics, Natural Science and Artificial Intelligence. He can be contacted at email: salem@cis.asu.edu.eg. He has more than one hundred research items that can be viewed at https://www.researchgate.net/profile/Mohammed_Abdel-Megeed_Mohammed_Salem